NOISE RADAR DESIGN

UDC 621.37

ULTRA-WIDEBAND PSEUDO-NOISE SENSORS

SACHS, J.; KMEC, M.; FRITSCH, H. C.; HELBIG, M.; HERRMANN, R.; SCHILLING, K.; RAUSCHENBACH, P.

The ultra-wideband (UWB) pseudo-noise (PN) technique merges the circuit simplicity of the pulse technique and the precision of the sine wave method with the LPI performance (low probability of intercept) of noise radar. Binary PN sequences of large bandwidth may be generated and captured with high precision and temporal stability by comparatively simple means. This opens up new high-resolution short-range radar applications. The article introduces the basic working principle, summarizes the state of recent devices, and introduces some key parameters as assistance for device parameterization that is appropriate for an intended application.

Keywords: ultra-wideband, pseudo-noise, M-sequence, Golay-sequence, sub-sampling, Hadamard-transform, impulse response function, frequency response function.

1. INTRODUCTION

The aim of this paper is to give an overview of the recent development state of ultra-wideband (UWB) sensing devices based on pseudo-noise (PN) codes. Since the radio emission of UWB devices is restricted by radio regulation to a very low power level, such sensors are typically found in short range applications, i.e. their range coverage is barely more than some tens or hundreds of meters.

The use of ultra-wideband PN-codes for stimulation of the test scenario brings some advantages, which will be summarized in what follows.

• Binary PN-codes such as an M-sequence have a crest-factor relatively close to unity. Hence, they carry a large amount of energy even if their magnitude is quite small. Thus, PN-codes provide best conditions for large suppression of random perturbations while protecting the sensor electronics and the test objects from strong electric fields. This is especially important, since one often deals with very near field measurements involving e.g. biologic tissue. Furthermore, it also enables monolithic integrated RF-circuits manufactured in a low-cost semiconductor technology.

• Some binary UWB PN-codes may be **easily generated** by high-speed digital shift registers with an appropriate feedback structure (for details on PN-sequences see [1]). The bandwidth of the sounding signal depends on the clock rate of the shift register. The generation of the wideband signal is controlled by a single tone RF-generator which pushes the shift register. Single tone generators can be built very precisely with respect to short time frequency fluctuations (phase noise) and with respect to the absolute frequency value (e.g. atomic clock as ultimate solution). In consequence, UWB-sensors based on PN-signals may have available very precise internal time reference if required. Firstly, this allows very precise range measurements due to the absolute frequency precision. Secondly, the sensors are very sensitive for weak range variations (often named micro Doppler) due to low phase noise of the timing reference. For details on corresponding aspects see [2].

• **PN-signals are periodic**. Hence, we can apply sub-sampling and synchronous averaging. Sub-sampling (stroboscopic sampling) will reduce the technical effort of data capturing and handling. Needless to say, that high sub-sampling factors must be traded against receiver efficiency leading to lower noise suppression or extended recording time (see [3] for comprehensive discussions). Consequently, one has to find a compromise between technical effort/device costs and degradation of measurement speed.

Synchronous averaging serves as noise suppression and reduction of data amount. It can be applied if the speed of data capturing is higher than required from the measurement scenario. The period length of the PN-code and capturing speed should be selected according to the requirements of the test scenario (see below for details). In order to reduce the data amount to be handled, the PN-code should be as short as possible.

Short sequences will however degrade the LPI (low probability of intercept) performance. In order to approach the LPI behavior of random noise, the PN-code and/or the clock rate of the shift register may be irregularly switched in time intervals comprising an integer multiple of periods.

The periodicity of the sounding signal avoids any truncation effects if appropriately captured. Furthermore, an expectation procedure for variance reduction as in case of random noise sounding signals is not necessarily required. Thus, the measurement approach is basically suited for high speed UWB-measurements.

• In case of radar applications, the **receive signals have to be compressed** in time in order to achieve an interpretable impulse response function. The impulse compression leads to a coherent energy accumulation of the measurement signal in favor of

random perturbations as additive noise, jitter, or jammers which are only non-coherently accumulated. Hence, an excellent suppression of various perturbation signals is inherent.

In what follow, we will start with a short introduction of the basic functioning of an UWB PN-sensor and we will summarize the key parameters of a PN-device in order to have some design guide lines for specific applications. In a further section, we will present a family of PN-devices for short range radar applications as well as general purpose time or frequency domain measurements. Finally, we will give an overview over some useful data pre-processing steps.

2. M-SEQUENCE PRINCIPLE

The design and technical implementation of an UWB-sensing concept should respect three key issues. These are the generation of the sounding signal, the capturing of the response signal, and the optimization of data throughput. We will discuss these points on the basis of Fig.1 which was firstly introduced by [4] and thoroughly analyzed in [3].

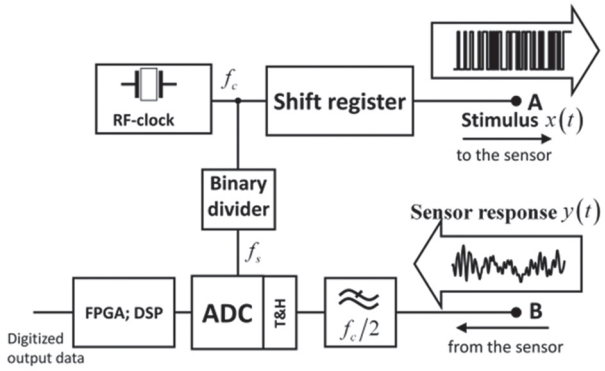

Fig. 1: Basic concept of UWB PN sensor head

The aim of this circuit is either the determination of the impulse response function (IRF) or the estimation of the frequency response function (FRF) related to the transmission path between the points A and B of Fig. 1. The measurement of the IRF is usually of interest in radar or TDR (Time Domain Reflectometry) operation mode, while the capturing of the FRF is applied in the network analyzer operation mode. Both methods only differ in the kind of processing the captured data.

The measurement of the IRF or FRF of a device or scenario under test requires a stimulation signal of sufficiently large bandwidth. In the simplest and most reliable case, one applies M-sequences (maximum length binary sequence). They are generated by linear feedback shift registers. Fig. 2 gives an example of one of its canonical structures. A second option would be the Fibonacci structure. It is not shown here since the Galois structure is usually preferred due to higher possible operational frequencies. The upper limit of the clock rate is determined by the toggle time of the individual flip-flops in the shift register and the delay of the feedback paths. In order to keep both as short as possible, the shift register must be monolithically integrated. A list of appropriate feedback structures is given in the online annex of [3]. The unit delay is provided by flip-flops which are pushed by an RF-clock $f_c = 1/t_c$. The state $Q_v(nt_c)$ of any flip-flop may act as the stimulation signal $x(t)$.

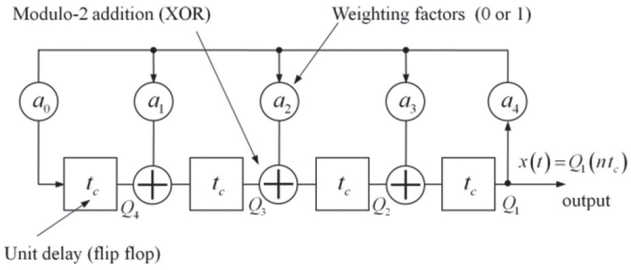

Fig. 2: Galois-structure of 4th order linear feedback shift register

Some characteristic functions – exemplified for an ideal M-sequence of 4th order – are depicted in Fig. 3. Time evolution and spectrum of a realistic M-sequence are shown in Fig. 4 and 5. The M-sequence is a periodic time signal having a discrete spectrum whose power envelope has a sinc^2-shape. Within the spectral band $[0, f_c/2]$, the stimulus power can be considered as nearly frequency independent which makes it suitable for IRF and FRF measurements of test objects having an operational band within this range. Above $f_c/2$, the signal power will rapidly decay so that random noise will more and more dominate the signal if the measurement bandwidth is extended beyond that limit.

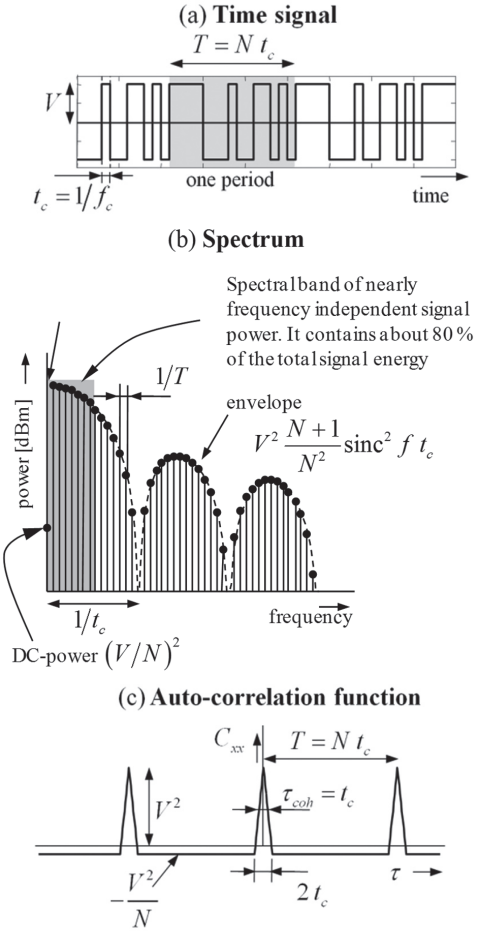

Fig. 3: Characteristic functions of the band unlimited M-sequence: time signal (a), power spectrum (b) and auto-correlation function (c)

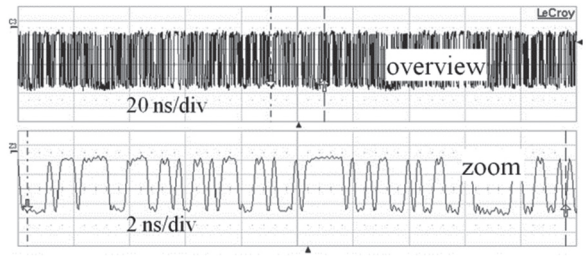

Fig. 4: Time evolution of a real M-sequence (9th order; clock rate 5 GHz). The clock rate was chosen to meet the bandwidth of the digital real-time oscilloscope

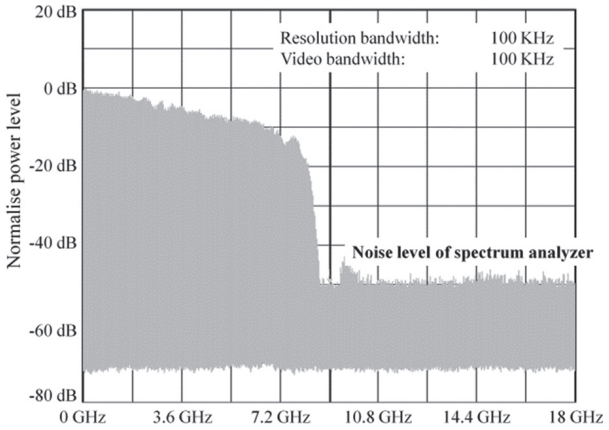

Fig. 5: Band limited spectrum of an M-sequence (9th order; clock rate 18 GHz)

The determination of the IRF $h(t)$ is based on the following relation:

$$C_{yx}(t) = h(t) * C_{xx}(t) \qquad (1)$$

in which $C_{xx}(t) = x(t) * x(-t)$ is the auto-correlation function of the stimulus and $C_{yx}(t) = y(t) * x(-t)$ represent the cross-correlation between receive signal and stimulus. The symbol $*$ means convolution. Obviously, the triangular shape of the auto-correlation function approaches a Dirac-delta with increasing clock rate of the shift register. Thus, we can roughly approximate for sufficiently large f_c: $C_{yx}(t) \sim h(t)$ (see also annex B9 of [3]).

The DC-offset of $C_{yx}(t)$ can mostly be ignored since we usually deal with AC-coupled systems and furthermore the DC-value of the measured signal is often affected by the offset voltage of the measurement receiver. If the DC-offset from $C_{xx}(t)$ is of importance, one can use complementary Golay sequences [3, 5-8] which will, however, complicate the device implementation – especially for a large bandwidth.

Since we like to process our data in the numerical domain, we first have to digitize the response signal $y(t)$. In order to relax the conditions to meet the Nyquist criterion, we apply sub-sampling. This is allowed since the response signal is periodic. Sub-sampling may drastically reduce the actual sampling rate as well as the data throughput and therefore it will decrease the device costs and the power consumption of the circuits.

A very simple and extremely stable approach to control the sub-sampling procedure follows from the band limitation to $f_c/2$ as depicted in Fig. 1 and Fig. 3 (b). For this case, the Nyquist criterion leads to a minimum (equivalent) sampling rate of $f_{eq}=f_c$, i.e. we only need one sample per chip of the PN-sequence whereat the capturing of these data points may be scattered over many periods of the response signal due to its periodicity (therefore the term "equivalent" sampling rate). The simplest way to control the data capturing exploits binary dividers (refer to Fig. 1). It assumes a signal length of $N = 2^m - 1$ chips (as valid for an M-sequence) per period. If we apply a binary divider of one stage, the actual sampling rate will be $f_s=f_c/2$ and we need two signal periods to capture the whole data set: the odd sample numbers during the first period and the even sample numbers during the second period. A binary divider of two stages reduces the sampling rate further to $f_s=f_c/4$. But now, we already need 4 periods to gather all data. This principle works for all orders of the binary divider.

In the case of Golay-sequences, the approach has to be slightly modified. The length of a Golay-sequence is 2^m which interdicts the use of a simple binary divider. If however the dividing factor is modified to $2^n \pm 1$, it works as before.

The use of the binary divider for sub-sampling control has some essential advantages:

- It provides very sharp trigger edges leading to sampling events which are robust against random jitter.
- The divider runs through all its states before it releases a new sampling event. Hence, any asymmetries of the internal flip flops will not affect the timing precision.
- The timing precision is determined by the single tone RF clock generator. If its frequency is stable within the recording time, the device internal time reference will be absolutely linear and stable. This guarantees very precise time measurements (also for long propagation times) and allows a practically unlimited number of synchronous averages for noise suppression when the test scenario/object is time invariant.
- The data capturing deals with Nyquist sampling. It provides the lowest possible data throughput which is required to correctly reconstruct waveform (in case of no prior knowledge). The visualization of a Nyquist sampled signal is less comprehensible for the human eye. Therefore, visualized waveform should be $\sin x/x$-interpolated for display. Note, non-ideal low-pass filters (namely due to their limited stop band attenuation) will cause some errors within the interpolated signal.

Except for the low-pass filter in Fig. 1, all device components may be monolithically integrated (compare Fig. 10 below). If one removes the analog RF-low pass, the involved electronic components will give a "natural" band limitation. Since it will certainly be beyond $f_c/2$, one has to increase the equivalent sampling rate – i.e. one has to take more than only one sample per M-sequence chip.

As depicted in Fig. 6, this can be achieved by a slight extension of the circuit from Fig. 1 [9]. The basic sampling approach remains the same as before. But it will be q-fold repeated whereat each time the sampling cycle is shifted by the q-th fraction of the clock period (i.e. $\Delta t_q=(qf_c)^{-1}$). This is managed with the additionally inserted steerable phase shifter.

By this approach, the equivalent sampling rate is increased to $f_{eq}=qf_c$ (which can be selected high enough to meet the Nyquist criterion if no artificial spectral cutting is applied) but also the recording time is extended by the factor of q. The captured noise power will also grow much stronger with increasing factor q than the energy of the response signal (due to the spectral decay of the stimulus signal). However, both effects may be neutralized, if the q-fold oversampled signal is band limited to $f_c/2$ by digital low-pass filtering now. This is quite more flexible but also requires more power for signal processing. With digital $f_c/2$ filtering, the same noise performance as a q-fold synchronously averaged signal from the basic concept according to Fig.1 with the analog low-pass filter can be obtained. Hence, the same recording time is needed for both cases. Since digital low-pass filtering may be joined with decimation, we will finally get the same data amount in both systems.

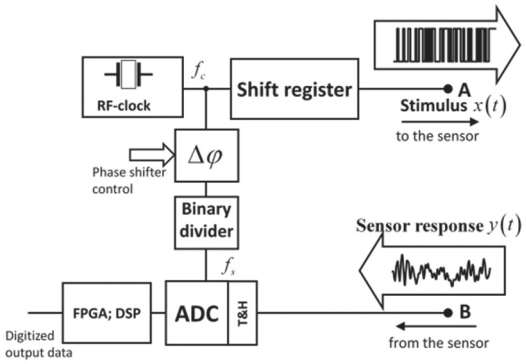

Fig. 6: Modified UWB PN-sensor head for equivalent time oversampling

3. ILMSENS PN-DEVICE LINE

Based on the working principle described in section 2, ILMsens develops a toolbox of wideband PN-devices and components for application-specific wideband measurements within the low-frequency, the radio frequency, and the microwave range. The intended scope of the toolbox is symbolized in Fig. 7. Herein, we distinguish between the baseband units which are the key component of every PN-device, the various options of RF-frontends and the basic software to operate the devices with standard computers.

The basic hardware structure is depicted in Fig. 8. It shows a baseband unit and an RF-frontend as two separated modules so that the sensor can be flexibly adapted to user requirements. The baseband unit constitutes from two parts, the RF-unit and a digital board containing the electronics for digitizing, high-speed pre-processing, and data transfer.

For the RF-unit, there are three realization options:

- The multi-chip RF-unit contains several custom-made SiGe-chips. This implementation provides high flexibility to modify the device structure concerning specific application requirements. Furthermore, it has the best RF-performance due to careful shielding between transmitter and receivers. An implementation example is shown in Fig. 9.
- In the case of the single-chip baseband unit shown in Fig. 10, the whole RF-part is merged in a single SiGe-chip while the digital board may be the same as before. This realization requires less supply power and less electronic components. Furthermore, the small size of the integrated RF-part – possibly including the RF-frontend, too – permits to place the measurement ports directly into the intended measurement plane. Hence, one can omit RF-cables. This will give additional degrees of freedom in the applicator design (antennas, coaxial probes, electrode configurations) since impedance matching is of less importance under this condition.
- The real-time baseband unit completely renounces the RF-part. Test signal generation and data capturing is entirely organized by the digital board which is identical for all three types of baseband implementation. Its bandwidth is mainly limited by the FPGA performance and the sampling rate f_s of the ADCs.

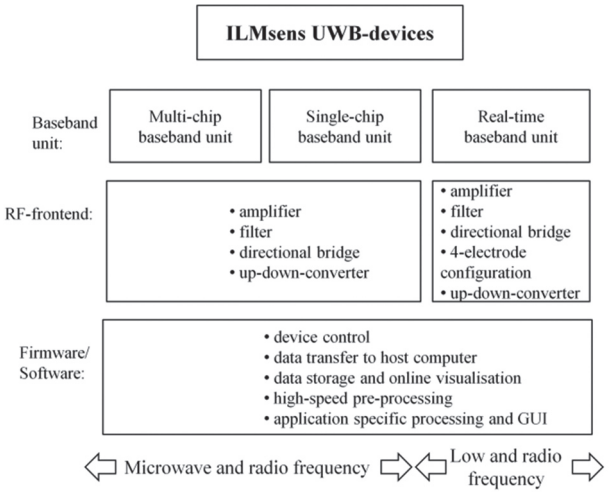

Fig. 7: PN-device toolbox

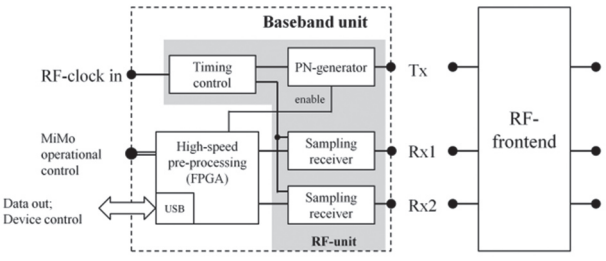

Fig. 8: Basic PN-device structure

Independent from the actual technical implementation, every baseband unit covers one PN-generator (which may be enabled or disabled during the operation of the measurement head) and two parallel working receiver channels. This configuration permits several measurement arrangements:

• The device may be operated as a wideband radar interferometer (e.g. used in Through-Wall-Radar) or as polarimetric radar.

• One channel may be used to capture the stimulus signal for reference.

• The device is able to capture one-port scattering parameters since it is able to stimulate a port and to measure the incident and emanating wave if directional bridges are inserted (see Fig. 10).

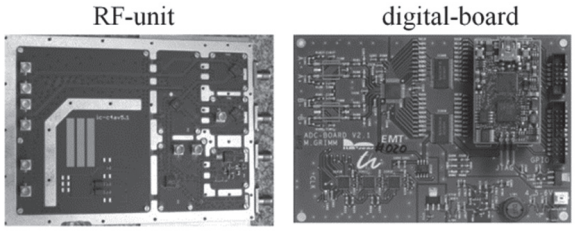

Fig. 9. Disassembled multi-chip baseband unit showing the RF-unit and the digital board which are stacked when in operation

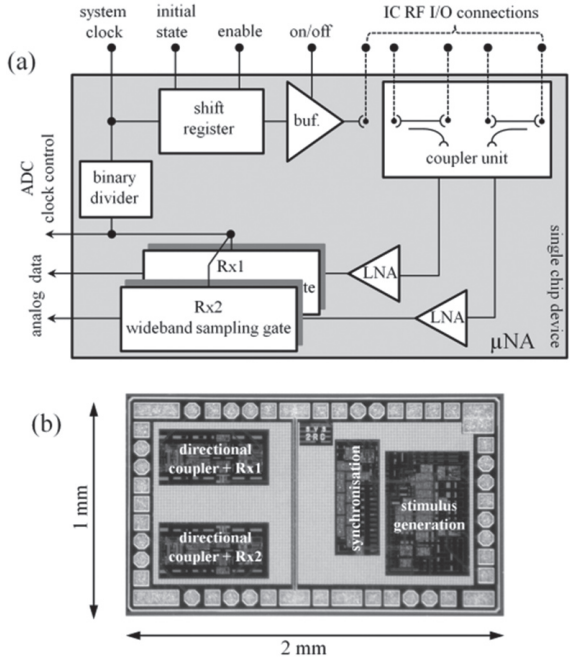

Fig. 10. Monolithically integrated M-sequence RF-unit with two reflectometer inputs: circuit schematic (a) and chip micrograph (b)

• The device is able to capture one-port impedance parameters since it is able to stimulate a port and to measure current and voltage.

• The device may act as a receiver only by disabling the PN-source.

• Several devices may be cascaded to form MiMo-Systems as depicted in Fig. 11. This permits the construction of MiMo-radars and multi-port S-parameter or Impedance-parameter measurement systems.

The optional RF-frontends provide the interface for application specific applicators or measurement circuits. They may contain filters, amplifiers, directional bridges, current-voltage converts, up-down-converters etc.

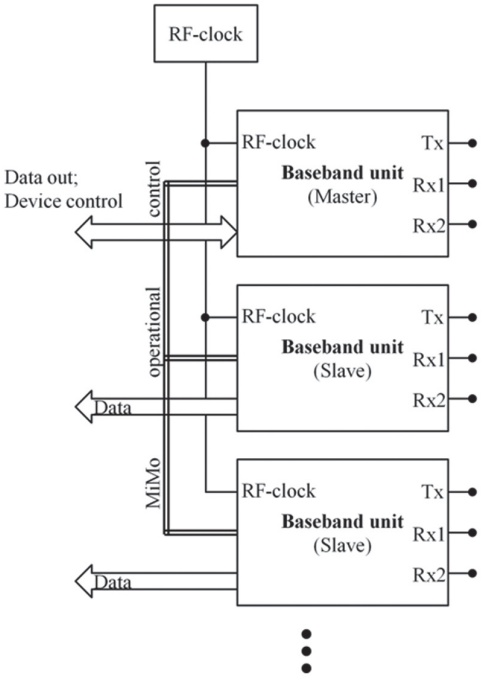

Fig. 11. MiMo-device structure

Fig. 12–16 exemplify implemented devices, their respective device extensions, and frontends.

Fig. 12. Standard baseband unit

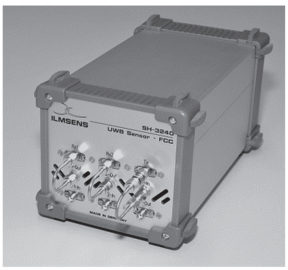

Fig. 13. FCC respectively ECC compatible device. These devises provide a complex valued IRF

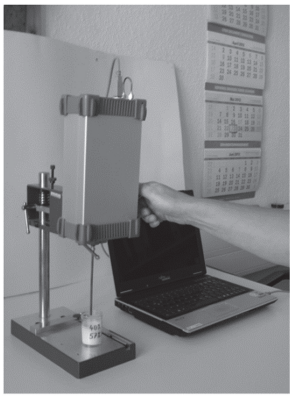

Fig. 14. Baseband unit extended with an active directional bridge for impedance spectroscopy and mono-static radar applications

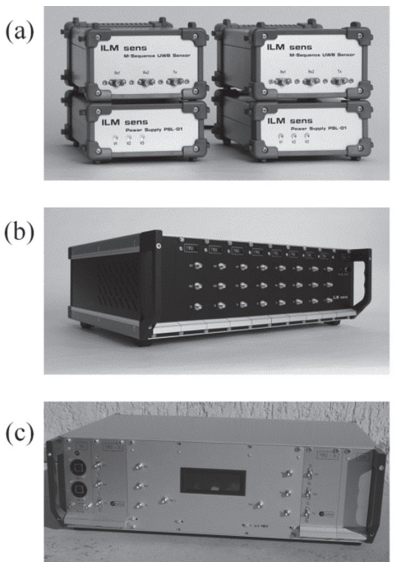

Fig. 15. Several options of MiMo-devices: (a) 2Tx/4Rx-system built from two basic modules. (b) 8Tx/16Rx-system. (c) 2Tx/4Rx-system with build-in reflectometers for scattering parameter measurements

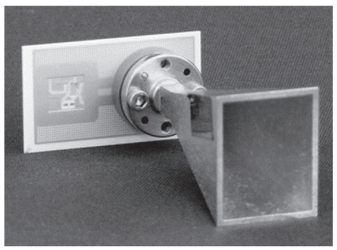

Fig. 16. Experimental wideband 60 GHz-frontend based on monolithically integrated SiGe-up-down converters extending the FCC-compatible PN-device for mm-wave channel sounding and radar [10]

The firmware to operate the devices pursues a corresponding modular concept as the hardware. Depending on the requirements and the skill of the user, two strategies are supported. In the first case – i.e. ultraANALYSER as shown in Fig. 17 – the software modules are designed to work stand alone for a set of well specified measurement tasks (e.g. short range radar and microwave imaging, Time Domain Reflectometry, vector network analyzer, impedance spectroscopy, ...). In the second case (see Fig. 18), the user has to implement the data processing on its own. Only the basic functionalities such as data transfer, data storage, device parameterization, and on-line visualization are available. Currently, it is based on MATLAB, but it will be extended to e.g. LabView in the future.

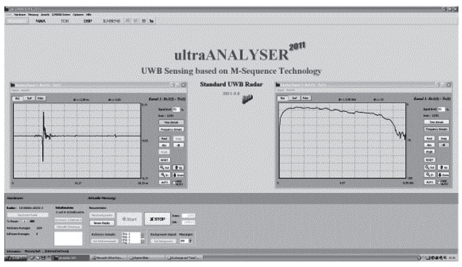

Fig. 17: ultraAnalyser GUI for standard stand-alone applications

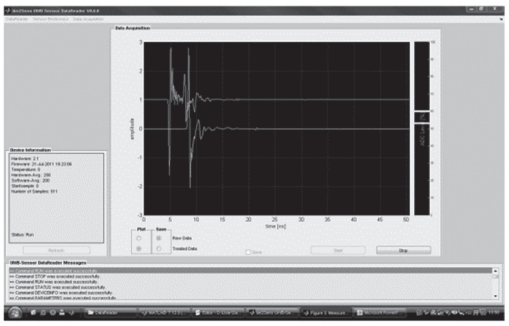

Fig. 18: MATLAB GUI for visualization, storage, and integration of a user function enabling user specific processing

4. KEY PARAMETERS

The most important quantities influencing the performance of a PN-sequence unit according to Fig. 1 are symbolized by the design tetrahedron in Fig. 19.

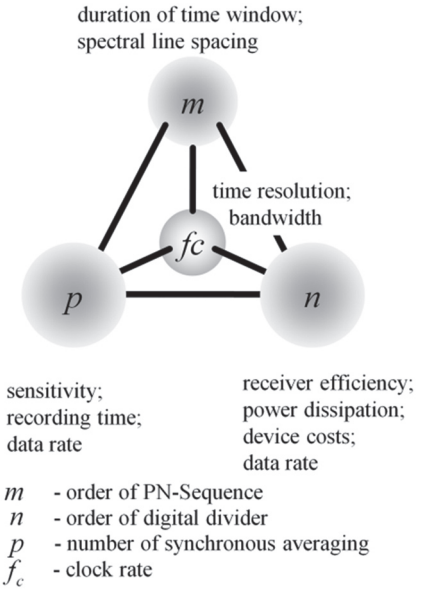

Fig. 19: Design tetrahedron of a PN-sequence system

Usually, one can select among four quantities to optimize the device performance for a specific application. These are the RF-clock rate f_c, the shift register length m, the length n of the binary divider and the number p of synchronous averaging. From this, we can roughly estimate the main features of the sensing unit (c_0 – speed of light; b – effective number of bits of the ADC and T&H):

Bandwidth:

$$B \cong 0 \cdots f_c/2 \tag{2}$$

Range resolution:

$$\delta_r \cong \frac{c_0}{f_c}. \tag{3}$$

Observation time window length:

$$T \cong \frac{2^m}{f_c}. \tag{4}$$

Spectral line spacing: $\Delta f = T^{-1} \cong 2^{-m} f_c$ (5)

Unambiguity range: $R \cong 2^{m-1} \frac{c_0}{f_c}$ (6)

Recording time per IRF or FRF:

$$T_R \cong \frac{p2^{m+n}}{f_c}. \quad (7)$$

Effective data amount per measurement:

$$H[\text{bit}] \cong \left(b + \frac{1}{2}\,\text{lb}\,p\right)2^m \quad (8)$$

(note, the word length of a data sample increases to $(b+\text{lb}p)$ bits by p-fold synchronous averaging. But half of the "new" bits are noise affected, so that finally the effectively utilizable resolution gain will be $(\text{lb}\,p)/2$ bit).

Effective bit rate for continuous operation:

$$R_b = \frac{H}{T_R} \cong \frac{2b + \text{lb}\,p}{p2^{n+1}} f_c. \quad (9)$$

Eq. (8) and (9) assumes that no time compression was performed. It would increase the word length per sample by m bit.

In case of non-stationary test scenarios, the maximum recording time is either restricted by the bandwidth of the scenario variations (i.e. $2B_{TS}T_R \le 1$ – Nyquist theorem of the test scenario) or by the Doppler Effect. The latter provokes de-correlation between transmitted and received signals for high speed targets. In order to keep the de-correlation negligible, the recording time should not exceed the maximum target speed of [3]:

$$v_{\max} \cong \frac{\delta_r}{T_R} \cong \frac{c_0}{p2^{m+n}}. \quad (10)$$

Please note, in the case of UWB PN-sequences, we will not observe Doppler ambiguity as is n the case for narrowband signals.

The dynamic range of the sampling receivers D_{R_x} is limited by different effects (see [3] for a detailed discussion). For the sake of shortness, we will refer only to limitations by electronic and quantization noise here. For time (superscript (TD)) and frequency (superscript (FD)) domain data, it can be approximated by:

$$\begin{aligned} D_{R_x}^{(TD)}[\text{dB}] &\cong 6b + 3m + 10\lg p \\ D_{R_x}^{(FD)}[\text{dB}] &\cong 6b + 10\lg p \end{aligned} \quad (11)$$

which leads to a recording time referred dynamic range (specific dynamic range DT) of:

$$\begin{aligned} D_{R_x}^{(TD)}[\text{dBs}] &= 10\lg(D_{R_x}^{(TD)}/T_R[\text{s}]) \\ &\approx 6b - 3n + 10\lg f_c[\text{Hz}] \\ D_{R_x}^{(FD)}[\text{dBs}] &= 10\lg(D_{R_x}^{(FD)}/T_R[\text{s}]) \\ &\approx 6b - 3(m+n) + 10\lg f_c[\text{Hz}] \end{aligned} \quad (12)$$

[dBs] – read dB per second; $D_{R_x}^{(\ldots)}$ – in linear scale.

The time domain related dynamic range refers the peak value of the time compressed signal to noise while the frequency domain related dynamic range compares the strength of an individual sine wave component with the noise power.

All these equations have shown the large room that exists to adapt the properties of the sensing device to the actual requirements. In standard configurations, the clock rate f_c is fixed to 125 MHz (real time unit only) or 5, 7, 9, 13, and 18 GHz for the RF units, respectively. The length m of the shift register is either 9 or 12 and the binary divider in our sensors is of order 9. The recently achieved specific dynamic range is about $DT^{(TD)} \approx 114$ dBs.

5. BASIC PRE-PROCESSING

Pre-processing is used to treat the captured data in such a way that it may be used by the subsequent main processing like microwave imaging, target detection, parameter extraction, and so forth. The pre-processing is mainly aimed at providing the IRF or FRF of the test object and at reduction of captured data volume to a manageable amount. The different procedures of pre-processing are distributed between the sensor internal processor (typically an FPGA and/or DSP) and the host computer. As long as the procedures deal with linear operations (e.g. correlation, Fourier transform, low-pass filtering, averaging, etc.), their sequence can be arbitrary selected due to the law of commutation. Hence, one is well advised to start with simple and fast procedures which additionally lead to a reduction of the data amount. Such procedures should run in the FPGA of the UWB-device in order to disburden the data interface to the host computer (e.g. USB2) which is often the bottleneck within the processing chain. Consequently, algorithms which increase the amount of data (e.g. time compression by correlation or imaging) should run after transmission to a computer. In what follows, some useful pre-processing approaches will be shortly summarized.

Data reduction by blind measurements: The minimum recording time of recent PN-sequence devices (which uses a 9th order binary divider for sampling control) ranges between 14 μs and 420 μs (i.e. about 2.400 to 71.000 response functions per second) depending on the clock rate and the order of the M-sequence (for details see datasheets at www.ilmsens.com). Usual Windows PCs may reliably handle only about 200 (9th order M-sequence) or 25 (12th order M-sequence) response functions per second. This gap may be bridged in the simplest case by ignoring most of the measurements. This approach will be the method of choice if the recording time is limited by physical reasons as e.g. for tracking of high speed targets (see eq. 10).

Data reduction by synchronous averaging: In most of the intended applications of UWB PN-sensors, the motions and variations of the scenario under test are slow compared to the measurement speed. Hence, we can increase the recording time. This opens up the opportunity to apply synchronous averaging by which the noise performance of the measurement will be considerably improved and additionally the data throughput will be reduced (refer to (8), (9), and (11)). If the required update rate of the measurements may be handled by the host computer, this approach will not cause any data losses.

Data reduction by background removal: in many cases, the UWB-sensor observes a scenario in which only minor variations appear (e.g. in case of through-wall radar, vital sign detection, supervision of a space etc.). Under such conditions, a new measurement will provide only minor new information. Therefore, the data amount can be drastically reduced by updating only the small variations of the captured data relative to the previous measurements. A simple realization of such background removal may be achieved by exponential filtering as expressed by (13).

$$\begin{aligned} \bar{y}_k(t) &= \alpha\, y_k(t) + (1-\alpha)\,\bar{y}_{k-1}(t) \\ \Delta y_k(t) &= y_k(t) - \bar{y}_{k-1}(t) \end{aligned} \tag{13}$$

Herein, $y_k(t)$ represents the captured signal of the k-th measurement cycle. $\bar{y}_k(t)$ is the background which is updated by every new measurement whereat the update speed is controlled by the forgetting factor $\alpha \in (0,1)$. The remaining signal $\Delta y_k(t)$ contains the variations (new information) gained by the k-th measurement. It has to be considered by the subsequent processing steps.

IRF and FRF determination: Typically the measurement should provide either the IRF (in case of radar or TDR) or the FRF (in case of the network analyzer operation mode) of the investigated transmission path. Since their calculation from the captured data is numerically more expensive than the previously mentioned procedures, it should be done at the end of the pre-processing chain. Depending on the required measurement precision, we have several options:

Option 1: Here, we assume that the sounding signal corresponds to an ideal M-sequence $m(t)$. That is, we disregard all deviations of a real M-sequence (as illustrated in Fig. 4 and 5) from the ideal one (as shown in Fig. 3). Under this condition, we can proceed as proposed by eq. (1), i.e. we calculate the cross-correlation between receiving signal and ideal M-sequence. The result can be interpreted as a first order approximation of the IRF of the transmission path:

$$h^{(1)}(t) \sim y(t) * m(-t) \tag{14}$$

Since the ideal M-sequence constitutes only from +1 or -1, the algorithm behind (14) can be implemented by a very fast and efficient way [3, 11]. It is called the fast Hadamard-transform (FHT) which has some structural similarity to the fast Fourier-transform (FFT). But in contrast to the FFT, it only requires summing and difference operations which can be handled extremely fast by modern FPGAs. The calculation of tens of thousands of IRFs per second should be feasible which could be applied to detect and track very fast objects. Note however, that (14) is linked with a time compression of the received signal which leads to an increased word length of the data (see also (8), (9) and related discussion). Therefore, the FHT should only run at the FPGA if it also performs target detection in order to reduce the data amount to be transferred.

Transforming $h^{(1)}(t)$ into the frequency domain, we would also get a first order approximation of the FRF $\underline{H}^{(1)}(f)$ of the device under test (DUT).

Option 2: This approach respects the actual time evolution or spectrum of the sounding signal. In order to get this signal, one either needs a second receiver for reference measurements or one performs a calibration measurement with a direct connection of generator and receiver (it is often called "response calibration" in network analyzer terminology). Now, we can de-convolve the actual sounding signal out of the captured one to get a better approximation of the DUT behavior. De-convolution can be done by several ways (see e.g. [12]). Here, we will only refer to a simple method which uses a frequency domain approach and a window function $w(f)$ for suppression of ill-conditioned parts of the spectrum. From this, we get a second order approximation of the DUT response in time or frequency domain.

$$\begin{aligned} & x(t) \xrightarrow{FFT} \underline{X}(f); \quad y(t) \xrightarrow{FFT} \underline{Y}(f) \\ & \underline{H}^{(2)}(f) = \frac{\underline{Y}(f)}{\underline{X}(f)} w(f) \xrightarrow{IFFT} h^{(2)}(t) \end{aligned} \tag{16}$$

Option 3: Unfortunately, option 2 of FRF or IRF determination does not respect all imperfections of the measurement device as e.g. cross-talk, port mismatch, multiple reflections etc. In order to remove these errors from the measurement, one needs a device calibration comparable to the approaches used for network analyzers. Deeper discussions of this topic would go beyond the scope of this article. But the interested reader can find the theoretic basis for network analyzer calibration in [13, 14] and corresponding considerations related to PN-devices including some examples are given in [3, 9, 15, 16].

The basic prerequisites to allow such error corrections are twofold. Firstly, one has to capture the complete set of signals at any port of the DUT, i.e. in case of S-parameter measurements one needs to know all ingoing waves a_n as well as all emanating waves b_n. Equivalently, one can also measure the current and the voltage at all ports. This is one of the reasons why ILMsens PN devices have two receive channels. The second assumption concerns the time stability of the measurement devices since their behavior must not change between repetitions of calibration and the time point of the measurement. Details of these issues are discussed in [2].

SUMMARY

The UWB PN-technique joins the circuit simplicity of the pulse technique and the precision of the sine wave method with the LPI performance of the noise radar. Binary PN sequences of large bandwidth may be generated by comparatively simple means. The selection of appropriate PN-codes depends on several aspects such as their auto-correlation and cross-correlation properties as well as the technical challenges of their generation. In order to determine a reliable estimation of the impulse response function of a DUT, the auto-correlation function of the PN-sequence should approach a Dirac-delta. This is best fulfilled by Maximum Length Binary Sequences

(M-sequence) and complementary Golay-codes. In both cases, the auto-correlation function represents a comb of triangular peaks having a base width of double the chip duration and a period according to code length. Hence, by increasing the code generating clock rate f_c, the wanted Dirac-delta is approximated better and better.

A family of M-sequence devices for high-resolution short-range sensing was introduced and the key parameters of the devices where summarized.

References

[1] H. J. Zepernick, and A. Finger, *Pseudo Random Signal Processing – Theory and Application*: John Wiley & Sons, 2005.

[2] J. Sachs, M. Kmec, and R. Herrmann, "Time and Range Accuracy of Short-Range Ultra-Wideband Pseudo-Noise Radar," in Noise Radar Technology, Yalta, Cremia (Ukraine), 2012.

[3] J. Sachs, *Handbook of Ultra-Wideband Short-Range Sensing - Theory, Sensors, Applications*, Berlin: Wiley-VCH, November 2012.

[4] J. Sachs, P. Peyerl, and M. RoЯberg, "A New Principle for Sensor-Array-Application.," in IEEE Instrumentation and Measurement Technology (IMTC), Venice (Italy), 1999, pp. 1390-1395.

[5] T. H. Andres, and R. G. Staton, "Golay Sequences," *Lecture Notes in Mathematics;Combinatorial Mathematics V*, C. H. C. Little, ed., Berlin, Heidelberg, New York: Springer, 1977.

[6] S. Foster, "Impulse response measurement using Golay codes," in Acoustics, Speech, and Signal Processing, IEEE International Conference on ICASSP '86., 1986, pp. 929-932.

[7] A. Vazquez Alejos, D. Muhammad, and H. Ur Rahman Mohammed, "Ground Penetration Radar Using Golay Sequences," in Region 5 Technical Conference, 2007 IEEE, 2007, pp. 318-321.

[8] A. V. Alejos, M. G. Sбnchez, I. Cuicas *et al.*, "Wideband Noise Radar based in Phase Coded Sequences," *Radar Technology*, G. Kouemou, ed.: InTech, 2010.

[9] R. Herrmann, "M-sequence based ultra-wideband radar and its application to crack detection in salt mines," Faculty of Electrical Engineering and Information Technology, Ilmenau University of Technology (Germany), Ilmenau, 2011.

[10] A. P. Garcia Ariza, R. Mьller, R. Stephan *et al.*, "60 GHz Polarimetric MIMO Sensing: Architectures and Technology," in EUCAP 2012, Prague, 2012.

[11] M. Cohn, and A. Lempel, "On fast M-sequence transforms (Corresp.)," *Information Theory, IEEE Transactions on,* vol. 23, no. 1, pp. 135-137, 1977.

[12] T. G. Savelyev, L. Van Kempen, and H. Sahli, "Deconvolution techniques," *Ground Penetrating Radar*, D. Daniels, ed., London: Institution of Electrical Engineers, 2004.

[13] D. K. Rytting, "Network Analyzer Error Models and Calibration Methods," in RF & Microwave Measurements for Wireless Applications (ARFTG/NIST Short Course Notes), 1996.

[14] D. K. Rytting, "Network Analyzer Accuracy Overview," in ARFTG Conference Digest-Fall, 58th, 2001, pp. 1-13.

[15] R. Herrmann, J. Sachs, and P. Peyerl, "System evaluation of an M-sequence ultra wideband radar for crack detection in salt rock," in International Conference on Ground Penetrating Radars (GPR), Ohio (Columbus), 2006.

[16] R. Herrmann, J. Sachs, K. Schilling *et al.*, "12-GHz Bandwidth M-Sequence Radar for Crack Detection and High Resolution Imaging," in International Conference on Ground Penetrating Radar (GPR), Birmingham, UK, 2008.

Manuscript received December, 20, 2012

Juergen Sachs is Senior Lecturer at Ilmenau University of Technology, Germany. He teaches "Basics of Electrical Measurement Technology", "Measurements in Communications" and "Ultra-Wideband Radar Sensing". He is head of several research projects, and inter alia coordinator of European projects for humanitarian demining and disaster relief. His research areas cover RF-signal analysis and RF-system identification; Surface Penetrating Radar for non-destructive testing and medical engineering, ultra wideband methods and their application in high resolution radar and impedance spectroscopy, digital processing of ultra wideband signals, array processing; and design and implementation of new RF device approaches.

Marko Helbig received the Dipl.-Ing. and Dr.-Ing. degrees in Electrical Engineering (Biomedical Engineering and Signal Processing) from Ilmenau University of Technology in 1996 and 2007. Currently, he is working as a research assistant at the Electronic Measurement Research Lab, Ilmenau University of Technology. His research interests include biomedical signal processing and high resolution ultra-wideband imaging for medical applications, especially for breast cancer detection.

Ralf Herrmann was born on 19.09.1978 in Germany. He started a course on engineering for computer science at the Ilmenau University of Technology in 1998 and graduated with an Eng. degree in 2004. After an internship at the Tohoku University in Sendai (Japan) he returned to Ilmenau in 2005 and has been working as a research assistant in the Electronic Measurement Research Lab of TU Ilmenau where he received his Dr. Eng. degree in 2011. Research focus is on system design of novel UWB pseudo-noise sensors and embedded electronics systems.

Martin Kmec received the Ing. degree in electronics and telecommunication technology from the Technical University Košice, Slovakia in 2000. In 2000 and 2001 he was with Meodat GmbH, Ilmenau, Germany, where his work has included the analysis and design of ultra-wideband current mode integrated circuits. Since 2001, he is with Electronic Measurement Laboratory on the Technical University Ilmenau in Germany as research assistant. His research interests are in the design and characterization of SiGe BiCMOS based circuits for novel UWB sensor systems. Hi is currently pursuing the Dr. degree in the field of monolithically integrated M-Sequence based UWB systems.

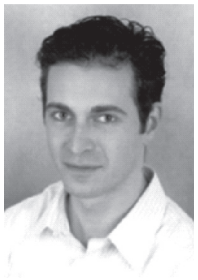

Kai Schilling received his diploma in Engineering Informatics with focus on Measurement and Telecommunication Technologies from Ilmenau University of Technology, Germany in 07/2007. He works since 08/2007 at the Institute for Information Technology Ilmenau as research assistant. His research activities cover the design and implementation of UWB Sensor Systems with focus on mixed signal and RF-hardware.

Peter Rauschenbach received his Eng. degree in electronics and telecommunication engineering from Ilmenau University of Technology, Germany in 1993. After his university studies, he was dealing with optical communication and microwaves. Since 1997, he is employee of MEODAT GmbH (Germany) where he is responsible for RF-technology, Filter and PCB design, and chip housing.

Hans-Christian Fritsch received the Master of Science in Business Informatics from Ilmenau University of Technology in 2010. In 2008 he completed the Bachelor of Science degree in Media Management. He is employed at the TU Ilmenau Service GmbH where he is charged with project management and the commercialisation of UWB-Technology.

УДК 621.37

Сверхширокополосные псевдошумовые сенсоры / Ю.Сакс, М. Кмец, Х.К. Фритч, М. Хелбиг, Р. Херрманн, К. Шиллинг, П.Раушенбах // Прикладная радиоэлектроника: науч.-техн. журнал. – 2013. – Том 12. – № 1. – С. 79–88.

Технология сверхширокополосных псевдошумовых (ПШ) сигналов объединяет простоту схем импульсной технологии и точность метода синусоидальных сигналов с низкой вероятностью перехвата шумовых радаров. Бинарные ПШ последовательности с широкой полосой могут быть достаточно просто сгенерированы и оцифрованы с высокой точностью и временной стабильностью. Это открывает новые применения радаров с высоким разрешением, работающих на малых дальностях. В данной работе описаны базовые рабочие принципы СШП ПШ радаров, приведен обзор новых устройств, представлены основные параметры как помощь в параметризации устройства, подходящего для применения метода.

Ключевые слова: сверхширокополосный, псевдошумовой, М-последовательность, последовательность Голай, субдискретизация, преобразование Адамара, импульсная функция отклика, амплитудно-частотная характеристика.

Ил. 19. Библиогр.: 16 назв.

УДК 621.37

Надшироковсмугові псевдошумові сенсори / Ю. Сакс, М. Кмец, Х.К. Фритч, М. Хелбіг, Р. Херрманн, К. Шиллінг, П.Раушенбах // Прикладна радіоелектроніка: наук.-техн. журнал. – 2013. – Том 12. – № 1. – С. 79-88.

Технологія надширокосмугових псевдошумових (ПШ) сигналів об'єднує простоту схем імпульсної технології і точність методу синусоїдальних сигналів з низькою імовірністю перехоплення шумових радарів. Бінарні ПШ послідовності з широкою смугою можуть бути досить просто згенеровані і оцифровані з високою точністю і стабільністю у часі. Це відкриває нові застосування радарів з високим розрізненням, працюючих на малих відстанях. У даній роботі описані базові робочі принципи СШП ПШ радарів, наведено огляд нових пристроїв, представлені основні параметри, як допомога в параметризації пристрою, придатного для застосування методу.

Ключові слова: надширокосмуговий, псевдошумовий, М-послідовність, послідовність Голай, субдискретізація, перетворення Адамара, імпульсна функція відгуку, амплітудно-частотна характеристика.

Іл. 19. Бібліогр.: 16 найм.